https://doi.org/10.5194/egusphere-2026-1712
Preprint. Discussion started: 15 April 2026

Future Changes in Severe Frontal Precipitation Events over Europe and Their Drivers

Armin Schaffer[1], Albert Ossó[1], and Douglas Maraun[1]
[1]Wegener Center for Climate and Global Change, University of Graz, Graz, Austria
Correspondence: Armin Schaffer (armin.schaffer@uni-graz.at)

Abstract.

Atmospheric fronts are closely linked to extreme precipitation across the mid-latitudes, which is projected to intensify in many regions under global warming. Understanding the physical drivers of these changes is essential to improve confidence in climate projections. Here, we analyze projected changes in seasonal heavy and extreme frontal precipitation events over Europe using the CMIP6 and EURO-CORDEX ensembles, combining event frequency analysis with frontal composite cross-sections to assess the changes of the underlying thermodynamic and dynamic processes. We find that the number of heavy frontal precipitation events increases by up to 50 % per degree of global warming, while extreme events are projected to more than double per degree. Large-scale circulation changes account for most regional reductions in frontal extremes, but contribute only weakly to the widespread increases. Thermodynamic changes, however, dominate the intensification of extremes. Increases in specific humidity are the primary driver of more intense events, while changes in the frontal circulation are minimal, likely because a more stable atmosphere counteracts potential strengthening from enhanced latent heat release.

1 Introduction

Extreme precipitation events have severe impacts on ecosystems, infrastructure, and societies, often leading to floods, landslides, and substantial economic losses (Field et al., 2012; Dottori et al., 2018; Coronese et al., 2019). These extremes are projected to intensify in many regions worldwide in response to global warming, driven by a combination of thermodynamic increases in atmospheric moisture and changes in circulation patterns (Trenberth et al., 2003; O'Gorman and Schneider, 2009; Westra et al., 2013; Shepherd, 2014; Pfahl et al., 2017; IPCC, 2023). However, reliably assessing how weather extremes will evolve remains a major scientific challenge, as thermodynamic and dynamic drivers can act in opposite ways and may either amplify or suppress extreme precipitation (Emori and Brown, 2005; Marotzke et al., 2017; Zappa et al., 2013). By first identifying the physical mechanisms underlying extreme events and then evaluating how accurately climate models represent these processes, confidence in projections can be increased and the reliability of regional impact assessments improved (Catto et al., 2010; Knutti et al., 2010; Maraun et al., 2017; Collins et al., 2018; Eyring et al., 2019). Process-based analyses, in particular, support this effort by clarifying how large-scale and mesoscale circulation and thermodynamic mechanisms contribute to the occurrence and intensity of extreme precipitation events (Boutle et al., 2011; O'Gorman, 2015).

https://doi.org/10.5194/egusphere-2026-1712
Preprint. Discussion started: 15 April 2026

In the mid-latitudes, a large fraction of extreme precipitation is associated with frontal systems, which are often accompanied by strong wind gusts that further amplify their impacts. In the current climate, approximately 60 – 90 % of extreme precipitation events in the mid-latitudes are related to fronts (Catto and Pfahl, 2013). Frontal precipitation is governed by processes operating across a wide range of scales, from mesoscale frontal dynamics to synoptic circulation (Bjerknes and Solberg, 1922; Browning and Monk, 1982; Browning and Pardoe, 1973). Hourly cold frontal extreme precipitation is highly dependent on a set of thermodynamic, synoptic, and mesoscale dynamic features (Schaffer et al., 2024). Climate models are generally able to capture these key frontal characteristics and their structure adequately, with higher resolution models improving the dynamic representation, which is especially beneficial for cold fronts and the associated precipitation. However, climate models exhibit notable biases in front frequency and the frontal heavy precipitation (Schaffer et al., 2025).

Observational and reanalysis-based studies have already indicated notable trends in frontal precipitation: over Europe, fronts characterized by strong thermal gradients, which are often linked to more intense precipitation, have become more frequent in recent decades (Schemm et al., 2017). At the same time, regional analyses have revealed spatially heterogeneous trends in frontal precipitation, likely associated with a poleward displacement of the storm track (Hénin et al., 2019). Only a few studies have investigated future projections of frontal systems and their impacts. For example, an analysis of CMIP5 RCP8.5 simulations reported a general decline in frontal activity across both northern and southern Europe (Catto et al., 2014). Other studies have found a considerable increase in frontal precipitation, based on a single model evaluation (Konstali et al., 2025), limiting the robustness of their conclusions. A comprehensive analysis of future changes in frontal precipitation has not been conducted, let alone an assessment of changes in the underlying physical drivers.

Here, we provide the first multi-model-ensemble-based analysis of frontal precipitation events under future climate conditions, with a focus on identifying the driving mechanisms of these changes. We begin by evaluating how the frequencies of frontal heavy precipitation events (HPEs) and extreme precipitation events (EPEs) change with warming. To determine the primary driver of these changes, we decompose the total change signals into thermodynamic and large-scale dynamic contributions. A key element of this study is the use of frontal composites to examine how the structure and mesoscale dynamics of frontal systems change in a future climate. By comparing composites from historical and future periods, we directly assess changes in moisture, circulation, and stability within frontal systems, providing a process-based evaluation of the mechanisms behind the increase in extreme frontal precipitation. These analyses address three main questions: How does the frequency of frontal heavy and extreme events change with warming? What is the relative importance of thermodynamic versus large-scale dynamic drivers? And how does the frontal structure respond to future warming?

2 Methods and Data

The methods applied in this study build on previous work on cold fronts (Schaffer et al., 2024) and have been extended to include the analysis of warm fronts (Schaffer et al., 2025). The following section provides an overview of all methods used, while detailed descriptions can be found in these earlier studies.

https://doi.org/10.5194/egusphere-2026-1712
Preprint. Discussion started: 15 April 2026

2.1 Data

We analyze 10 GCMs from the CMIP6 ensemble (Eyring et al., 2016) and 9 RCM simulations from EURO-CORDEX (Jacob et al., 2014) for the historical period 1970 – 2005 and the future period 2065 – 2100. The future CMIP6 simulations are based on the SSP5-8.5 scenario, while the EURO-CORDEX simulations follow the corresponding RCP8.5 scenario. These high-emission scenarios are selected to capture a strong climate change signal and to explore the upper range of plausible future climate responses. Within the EURO-CORDEX ensemble, two RCMs are driven by four and five GCMs from the CMIP5 ensemble (Taylor et al., 2012). All simulations providing the necessary 6-hourly, three-dimensional fields of temperature, humidity, wind, geopotential height, and precipitation from the ensembles have been selected. A complete list of all models used is provided in Table S1.

2.2 Front Detection

Fronts are identified using an objective scheme based on thermal gradients, following established methods (e.g., Hewson, 1998; Jenkner et al., 2009; Hewson and Titley, 2010). Specifically, we detect fronts from the smoothed equivalent potential temperature gradient ($\nabla\theta_e$) at 850 hPa. While potential temperature (θ) is commonly used in a strictly dynamical framework, θ_e is better suited for identifying frontal zones in moist, non-adiabatic conditions and has therefore been widely adopted in previous studies (e.g., Schemm et al., 2017; Hénin et al., 2019; Rüdisühli et al., 2020; Konstali et al., 2025).

To account for model-dependent variability and climate change effects, the $\nabla\theta_e$ threshold is computed separately for each model and period (historical and future) as the seasonal mean plus one standard deviation over a North Atlantic reference region (20°W–12°W, 40°N–58°N). This ensures a comparable number of detected fronts between periods and emphasizes spatial changes in frontal occurrence.

Frontal locations are defined as grid points with maximum $\nabla\theta_e$ where the Thermal Front Parameter (TFP) approaches zero:

$$\mathrm{TFP} = -\nabla|\nabla\theta_e| \cdot \frac{\nabla\theta_e}{|\nabla\theta_e|} \tag{1}$$

This method avoids explicitly identifying TFP maxima, which can introduce inconsistencies from higher-order derivatives, especially at higher resolution.

Detected points are classified using the cross-frontal wind component (u_f), distinguishing cold fronts ($u_f > 1.5\ \mathrm{m\ s^{-1}}$) and warm fronts ($u_f < -1.5\ \mathrm{m\ s^{-1}}$), while fronts with weaker u_f are discarded. Frontal points are then aggregated into continuous features, and only systems exceeding 500 km in length are retained. Additional filters are applied to remove non-synoptic frontal features. For cold fronts, we exclude cases where the angle between $\nabla\theta_e$ and the geopotential height gradient exceeds 120°, which removes spurious coastal and orographic boundaries. For warm fronts, we require a positive potential temperature difference between points 300 km ahead and behind the front to eliminate false detections associated with strong humidity gradients near warm conveyor belts (Schaffer et al., 2025).

https://doi.org/10.5194/egusphere-2026-1712
Preprint. Discussion started: 15 April 2026

2.3 Frontal frequency and precipitation

A circular area of 300 km around each frontal point is defined as frontal area. These areas are used to compute the front frequency (Fig. S1), as well as the frontal precipitation. Precipitation is considered frontal if it occurs within the defined frontal area. We further classify precipitation as heavy (extreme) if the 6-hourly total exceeds the historical 99.5th (99.95th) percentile at each grid point, corresponding to a 50 (500) day return period. If precipitation falls within the 300 km radius of both front types, it is split between cold and warm fronts. In such cases, precipitation is partitioned proportionally to the number of grid points associated with each front type. The total frontal precipitation is computed by adding up the precipitation for each front type. The number of frontal events is computed by summing the occurrence of events exceeding the thresholds.

To ensure comparability among models, the differences between the historical and future period are normalized by the projected global mean 2 m surface temperature change (ΔGMST). In the case of CORDEX, ΔGMST of the driving CMIP5 models are used. We chose GMST over local temperatures to avoid introducing artificial variations arising from spatial differences in local warming. Moreover, because frontal systems are synoptic-scale phenomena, the associated air masses may originate from regions far from areas affected by the fronts. Using ΔGMST allows us to evaluate changes in the number of heavy and extreme precipitation events relative to a given level of global warming, providing a consistent framework to compare responses across models and ensembles. ΔGMST values for DJF and JJA for each model are presented in Table S1.

2.4 Decomposition into large-scale drivers

To decompose the changes in frontal EPEs into the thermodynamic and large-scale dynamical contribution, the frequency of frontal EPEs is expressed as

$$N_{\mathrm{EPE}} = N_{\mathrm{FF}}\, p, \tag{2}$$

where N_{FF} is the front frequency and p is the conditional probability that a front causes an EPE. This formulation separates changes in the frequency of frontal systems from changes in their conditional severity. The total change in EPE frequency between the historical (h) and future (f) period is

$$\Delta N_{\mathrm{EPE}} = N_{\mathrm{FF}}^{\mathrm{f}}\, p^{\mathrm{f}} - N_{\mathrm{FF}}^{\mathrm{h}}\, p^{\mathrm{h}}. \tag{3}$$

Expanding this expression yields

$$\Delta N_{\mathrm{EPE}} = N_{\mathrm{FF}}^{\mathrm{h}}\, \Delta p + p^{\mathrm{h}}\, \Delta N_{\mathrm{FF}} + \Delta N_{\mathrm{FF}}\, \Delta p, \tag{4}$$

where the first term represents the thermodynamic contribution, that is, the increased probability of frontal EPEs occurring, while keeping the front frequency at the historical level. The second term represents the contribution from changes in the frequency of frontal systems, keeping the probabilities at historical values. The third term quantifies nonlinear higher-order interactions, typically small in magnitude. The three terms sum exactly to the simulated total change in EPE frequency. A comparison of the first two terms provides a clear diagnostic of the dominant mechanism. A similar analysis was presented by Crawford et al. (2025) for precipitation trends of northern hemisphere cyclones.

https://doi.org/10.5194/egusphere-2026-1712
Preprint. Discussion started: 15 April 2026

Because the front frequency changes potentially mainly depict the change signal in weak fronts, which do not cause EPEs, we also performed the analysis with respect to the change in HPE frequency N_{HPE}. Fronts causing HPEs are more likely to be able to cause EPEs, quantifying the frequency change in a more meaningful way. However, HPEs are defined using a historical percentile threshold. This term thus includes both large-scale dynamical changes in frontal activity and thermodynamic threshold-crossing effects that cause additional events to exceed the HPE threshold. We therefore interpret this term as a mixed contribution of large-scale dynamical changes and thermodynamic amplification of HPEs. For completeness, this analogous decomposition method using frontal HPE frequency is provided in Fig. S2.

2.5 Frontal composites

Frontal composites are constructed to represent the structure of the most intense frontal systems using a targeted sampling approach. For each frontal object, precipitation is characterized based on its most active segment. Frontal grid points are ranked according to standardized precipitation (anomalies normalized by their standard deviation), and the subset corresponding to approximately 200 km of frontal length is selected. The mean precipitation of these points is then used to represent the intensity of the frontal object, ensuring comparability across models with different resolutions and front geometries.

To avoid repeated sampling of the same system, only one frontal object per 24-hour period is retained. From this subset, the top 10 % of events are selected for compositing. The analysis focuses on three European regions: Northwestern Europe (48°N–61°N, 12°E–3°W), Southwestern Europe (36°N–48°N, 11°E–4°W), and Central Europe (48°N–58°N, 3°W–25°W). Frontal events from all regions are pooled into a single dataset prior to composite calculation.

For each selected event, a 1200 × 1200 km domain centered on the frontal system is extracted. The reference position is defined by the frontal point with median standardized precipitation among the selected high-intensity segment, which reduces sensitivity to frontal endpoints and occlusion regions. Fields are rotated into a front-relative coordinate system and interpolated onto common pressure levels (925–200 hPa at 25 hPa intervals) before averaging.

To examine front-relative dynamics, atmospheric fields are further decomposed into synoptic- and mesoscale components using a spectral filter. A low-pass scale of 1500 km and a transfer-function width of 500 km are applied, such that wavelengths above roughly 1000 km represent the synoptic-scale flow, while smaller scales are attributed to mesoscale variability. This decomposition is performed for each event prior to compositing.

3 Results

3.1 Change in frontal precipitation events

To assess how the frequency of frontal precipitation events changes under a warming climate, we first examine the projected number of frontal HPEs across Europe and the North Atlantic. In DJF, the number of events increases markedly in a zonal band across the North Atlantic and Europe (Fig. 1a – d). North and south of this band, a weak decrease is observed. Maximum increases exceed 50 % K^{-1} in CMIP6 and 40 % K^{-1} in CORDEX for cold fronts. Changes in warm frontal events follow

https://doi.org/10.5194/egusphere-2026-1712
Preprint. Discussion started: 15 April 2026

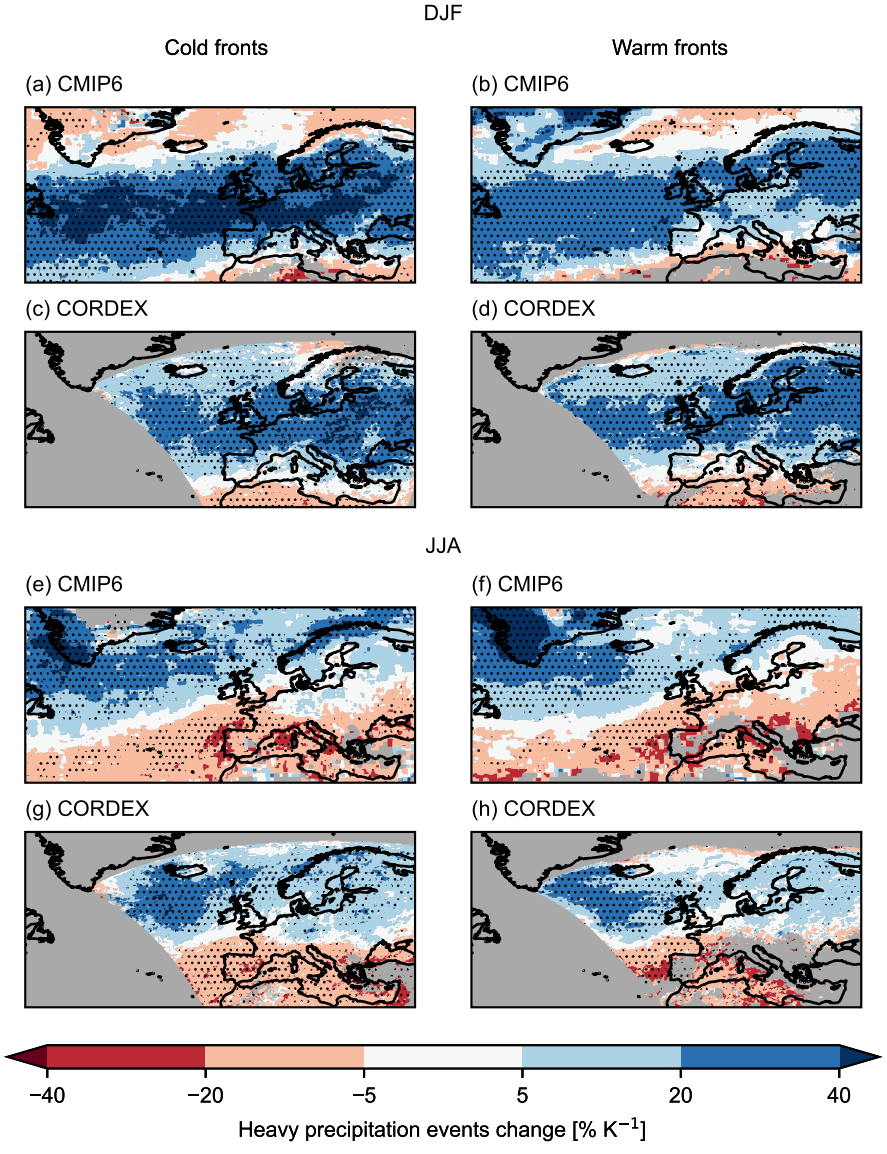

Figure 1. Relative changes in the number of frontal HPEs per degree of ΔGMST, for DJF (a – b) and JJA (e – h), for cold (a, c, e, g) and warm fronts (b, d, f, h). Panels (a, b, e, f) display CMIP6 and panels (c, d, g, h) the CORDEX averages. Stippling indicates areas where at least all but one model agree with the sign of the change. Areas are shaded gray if the fraction of frontal events relative to total events is below 10 % in the historical period or if they lie outside the EURO-CORDEX domain.

150 similar spatial patterns, but with lower magnitudes (up to +30 % K^{-1}). In JJA, a pronounced northward shift occurs, with more events over northern Europe and a decrease over the southern half of the domain (Fig. 1e – h). Both front types show consistent patterns in CMIP6 and CORDEX, although CORDEX exhibits a slightly weaker northward shift and an increase

https://doi.org/10.5194/egusphere-2026-1712
Preprint. Discussion started: 15 April 2026

in the Norwegian Sea. These patterns are broadly consistent with projected changes in the storm track (Simpson et al., 2014; Harvey et al., 2020; Priestley and Catto, 2022; Ossó et al., 2024). The weaker signal in CORDEX is consistent with the lower storm track sensitivity of the driving CMIP5 compared to CMIP6.

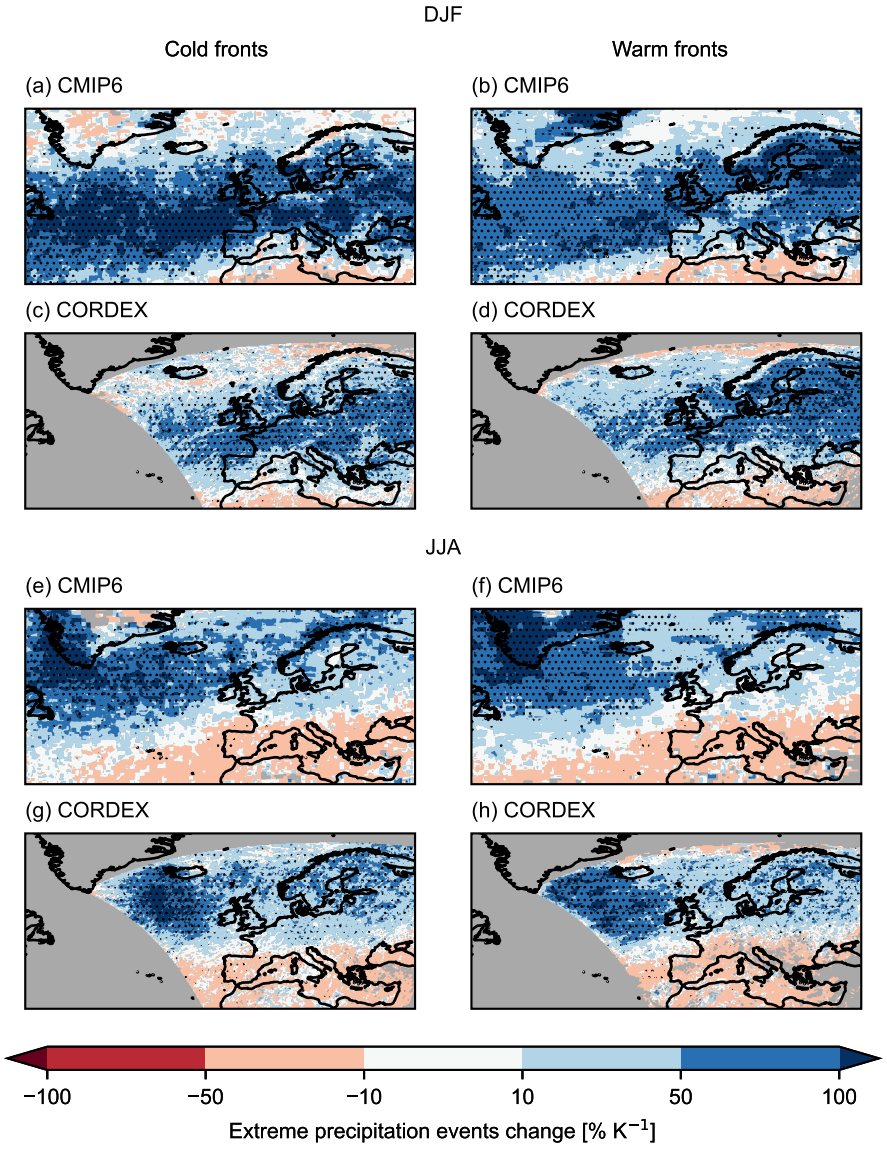

Figure 2. Same as Fig. 1, but for extreme frontal precipitation events.

The changes in the number of EPEs events exhibit seasonal patterns similar to those of heavy events (Fig. 2). However, the increases are roughly 2 – 3 times larger, with peak values for cold frontal EPEs exceeding 130 % K^{-1} in CMIP6 in some

https://doi.org/10.5194/egusphere-2026-1712
Preprint. Discussion started: 15 April 2026

regions. In JJA, some regions (e.g., France and Central Europe) show a reversal in the sign of change, with frontal HPEs decreasing while EPEs increase (Fig. 2e – h).

The large relative increase in frontal EPEs partly reflects their rarity in the historical period, as even modest shifts in the precipitation distribution can substantially raise extreme-event frequencies (Folland et al., 2001). The differing sign of change in frontal EPEs and HPEs in some regions indicates that the intensification reflects more than a simple shift of the precipitation distribution. To further demonstrate this, changes in the 99.5th and 99.95th percentiles of frontal 6-hourly precipitation are compared (Figs. S3, S4). In most regions and seasons, the higher percentile increases more strongly, indicating that nonlinear effects contribute to the increase in frontal EPEs.

3.2 Decomposition of frontal extreme precipitation event changes

To assess whether the strong increase in the number of EPEs is driven by thermodynamic effects or by changes in the large-scale circulation, we decompose the EPE change signal into three components: (i) a thermodynamic contribution, (ii) a front frequency contribution, and (iii) a residual term capturing higher-order interactions (Fig. 3).

The decomposition shows that the thermodynamic contribution dominates the increase in frontal EPEs across most regions and in both seasons, with particularly strong amplification along the storm-track. In contrast, regions with decreasing EPE frequency, e.g. the northern part of the domain in DJF and southern and eastern Europe in JJA, are primarily driven by front frequency changes, consistent with large-scale dynamical weakening of frontal activity. In JJA, parts of the Mediterranean and the Iberian Peninsula depict a decreasing effect of the thermodynamics, possibly related to drier conditions in this region (Feng and Fu, 2013; Scheff and Frierson, 2012; Liu et al., 2022). The residual remains small everywhere, confirming that the decomposition captures the main effects. Using HPE frequency instead of front frequency in the decomposition (Fig. S2) yields consistent results and further reinforces the conclusion that thermodynamic changes primarily drive the increase in frontal EPEs. To identify the physical processes underlying this dominant thermodynamic forcing, changes in frontal conditions and dynamic structure are assessed next using composite cross-sections.

3.3 Composites

Composite cross-sections provide the key mechanistic insight into how thermodynamic and dynamical processes shape future changes in frontal precipitation. They reveal how warming modifies moisture availability, static stability, and the circulation within frontal systems, thereby explaining why thermodynamic effects dominate the response of heavy and extreme events. To account for the strong resolution dependence of frontal dynamics (Schaffer et al., 2025), the CMIP6 ensemble is divided into low-resolution (CMIP6-LR) and high-resolution (CMIP6-HR) subsets. We focus on mechanisms that strongly influence precipitation and exhibit robust changes in a warmer climate, with additional Figures provided in the Supplementary Information.

The red and blue frontal lines drawn in the following figures (Figs. 4 – 9) are based on the TFP of θ_e zero contour lines. These lines strongly depend on the gradient of specific humidity, and thus on the amount of humidity in the warm air sector. In JJA the amount of humidity within the lifting area is greatly increased and therefore its gradient dominates the total $\nabla\theta_e$. As a consequence, the TFP zero contours are more upright and tend to not follow the classical backwards bend in cold fronts and

https://doi.org/10.5194/egusphere-2026-1712
Preprint. Discussion started: 15 April 2026

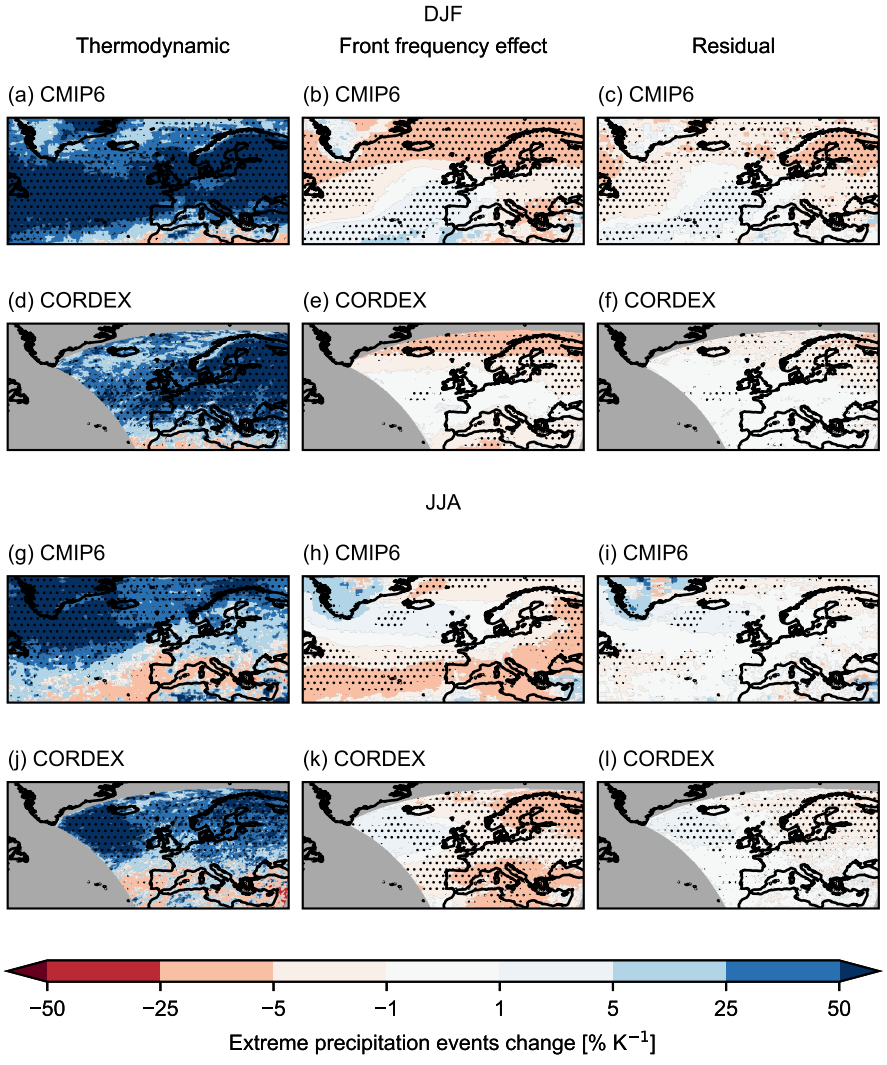

Figure 3. Decomposition of relative change in the number of frontal extreme precipitation events. The panels show the total EPE change (as in Fig. 2) expressed as the sum of thermodynamic (a, d, g, j), front frequency effect (b, e, h, k), and residual contributions (c, f, i, l) for both front types combined. The decomposition is based on expressing frontal EPE frequency as $N_{\mathrm{EPE}} = N_{\mathrm{FF}}\, p$, where N_{FF} is the number of fronts and p is the conditional probability that a front produces an EPE. Changes in EPEs can therefore be separated into (i) changes in p (thermodynamic contribution), (ii) changes in N_{FF} (large-scale dynamical contribution), and (iii) a small nonlinear residual term.

forward slope in warm fronts. These lines are not meant to perfectly represent frontal boundaries in a meteorological sense, but as guidelines to better understand the relative position of the detected fronts.

Atmospheric moisture is a key predictor of frontal precipitation, as sufficient humidity is a necessary precondition for the formation of heavy rainfall (Doswell et al., 1996; Schaffer et al., 2024). Across both cold and warm fronts the specific humidity

https://doi.org/10.5194/egusphere-2026-1712
Preprint. Discussion started: 15 April 2026

increases substantially in the warm sector. Low-level warm air specific humidity rises from $5-7$ g kg^{-1} by $0.3-0.5$ g kg^{-1} K^{-1} in DJF and from $7-10$ g kg^{-1} by $0.5-0.7$ g kg^{-1} K^{-1} in JJA (Fig. 4), broadly consistent with Clausius-Clapeyron scaling of 7 % K^{-1}. Within the cold air sector absolute specific humidity also exhibits increases, especially at lower levels, but less strongly. However, the relative increases similarly follow the Clausius-Clapeyron scaling.

Relative humidity change patterns differ between seasons. In DJF, relative humidity remains nearly unchanged (Fig. 4 g–ł), whereas in JJA it decreases markedly in the upper troposphere (Fig. 4 g–ł), especially in CORDEX. This reflects a slower increase in specific humidity compared to saturation vapor pressure, possibly due to limited moisture supply (Byrne and O'Gorman, 2016). The resulting upper-tropospheric drying may influence cloud formation and precipitation efficiency. A detailed figure of the relative humidity change is provided in the Supplementary Information (Figs. S5, S6). To assess whether the reduction in relative humidity occurs consistently across all analyzed regions (NWEUR, SWEUR, and CEUR), we further compare the change signals for each region individually (Figs. S7 – S12). While southwestern Europe exhibits the strongest decrease in relative humidity, the other two regions show comparable declines, particularly in the CORDEX ensemble, indicating a general trend toward relatively drier conditions over Europe in JJA.

These humidity changes also interact with modifications in atmospheric stability, further influencing frontal ascent. Across all composites and both seasons, upper-tropospheric warming is pronounced, particularly in the warm sector (Fig. 5). The temperature difference between 300 hPa and 850 hPa increases by roughly 0.9 K K^{-1}, reflecting moist-adiabatic adjustment of the vertical temperature profile. These values are roughly consistent in all models and seasons, highlighting a general increase in static stability. As a consequence, convection within the frontal zone could be dampened, reducing the potential for heavy and extreme precipitation.

Despite these substantial thermodynamic changes, the horizontal potential temperature gradient ($\nabla\theta$) across the front remains largely unchanged (Figs. S7, S8). In contrast, the equivalent potential temperature gradient ($\nabla\theta_e$) strengthens (Figs. S9, S10), reflecting the stronger differential increase in moisture between the warm and cold air masses (Fig. 4) rather than a change in dry temperature gradients.

Given the substantial increase in specific humidity within the frontal environment, corresponding changes in mesoscale circulation driven by enhanced latent heat release could be expected. However, the composites show only minor dynamical changes. Mesoscale convergence (Figs. 6, 7) and vorticity (Figs. 8, 9), which are both strongly linked to frontal precipitation intensity through convection (Schaffer et al., 2024), exhibit no systematic strengthening under future warming. In JJA, both cold and warm fronts even show a weakening of mesoscale circulation, consistent across all model subsets (Figs. 6, 7 g–l). The enhanced static stability likely counteracts any intensification of vertical motion associated with increased latent heating, aligning with the weak changes in mesoscale circulation.

On the synoptic scale, a key driver of frontal precipitation variability is the warm conveyor belt (Schaffer et al., 2024). Located ahead of the cold front and ascending over the warm front, this air stream transports warm, moist air toward and upward within the frontal zone (Browning and Pardoe, 1973; Browning, 1990; Heitmann et al., 2024), a process strongly connected to intense precipitation in fronts (Catto et al., 2015). To quantify this inflow, we analyze along- and cross-frontal wind components. Despite projected reductions in storm track activity, the composites show no substantial changes in these

https://doi.org/10.5194/egusphere-2026-1712
Preprint. Discussion started: 15 April 2026

synoptic air streams in either cold or warm fronts (Figs. S17 – S20). Minor reductions in the upper- and low-level jet speed can be seen in the CMIP6 simulations in JJA consistent with the reduction of jet activity in this season over central and southern Europe (Simpson et al., 2014; Ossó et al., 2024).

4 Conclusion

In this study, we investigated projected changes in heavy and extreme frontal precipitation events over Europe using CMIP6 and EURO-CORDEX ensemble simulations. We combine an analysis of event frequency changes with frontal composite cross-sections to assess the relative strength of large-scale dynamical and thermodynamic forcing, and to identify the processes within the frontal structure and mesoscale circulation that drive these changes.

Frontal HPEs are projected to increase notably in DJF across a zonal band from the North Atlantic into central Europe, with weak decreases north and south of this band. In JJA, a pronounced northward shift in events occurs, with increases over northern Europe and decreases across the southern half of the domain. These patterns are consistent with projected changes in the storm track (Simpson et al., 2014; Harvey et al., 2020; Priestley and Catto, 2022; Ossó et al., 2024). Frontal EPEs follow similar spatial patterns, but exhibit substantially larger relative increases. In JJA, some regions show a divergence between frontal HPE and EPE trends, with heavy events decreasing while extremes increase. A previous study of CESM2-LE simulations found comparable increasing trends in frontal precipitation, while non-frontal precipitation stagnates or even decreases in some regions (Konstali et al., 2025).

Our analysis shows that the strong increase in frontal EPEs is primarily driven by thermodynamic changes. While changes in the large-scale circulation also influence EPE occurrence and are the main driver of decreases in EPEs, namely in Northern Europe in DJF and Southern Europe in JJA, thermodynamic effects dominate the overall response. Similar results have been found when looking into precipitation trends of northern hemisphere cyclones (Crawford et al., 2025). Minor decreasing thermodynamic effects in southern Europe could be related to a future reduction in humidity in this region (Feng and Fu, 2013; Scheff and Frierson, 2012; Liu et al., 2022). These results identify thermodynamic mechanisms as the primary driver of future increases in the frequency of severe frontal precipitation events.

Frontal composite cross-sections show how these thermodynamic and dynamical forcings shape the frontal structure and circulation. Specific humidity increases substantially ahead and behind the front, consistent with Clausius–Clapeyron scaling. In contrast, relative humidity in JJA decreases in all analyzed regions in the upper troposphere, most notably in CORDEX simulations, indicating enhanced upward moisture transport but limited moisture supply over the continent, consistent with previous model-based findings (Byrne and O'Gorman, 2016). Observational trend studies show that such reductions in near-surface moisture have not occurred in the recent climate (Simpson et al., 2024), suggesting that the projected drying reflects conditions that may emerge only under stronger future warming.

Enhanced static stability, with the upper troposphere warming more rapidly than lower levels, is consistently observed across all models. The horizontal potential temperature gradient across the frontal boundary remains largely unchanged. Equivalent potential temperature gradients, however, strengthen due to differential moisture increases of the warm and cold air, highlight-

https://doi.org/10.5194/egusphere-2026-1712
Preprint. Discussion started: 15 April 2026

ing the dominant role of moisture in amplifying frontal intensity. Frontal circulation, reflected in mesoscale convergence and vorticity, shows no consistent changes in DJF, suggesting a balance between latent-heating–driven strengthening and the stabilizing influence of increased static stability. In JJA on the other hand, decreases in the frontal circulation can be seen. Together with the findings of decreased relative humidity, the effect of increased static stability seems to be stronger than the effect of increased latent heat release, potentially damping frontal precipitation in some regions. Larger-scale air streams, like the warm conveyor belt, remain stable, suggesting that the observed intensification of frontal precipitation is primarily thermodynamically driven rather than dynamically forced. Overall, these combined thermodynamic and minor dynamic adjustments lead to more intense frontal precipitation events across most of Europe.

In conclusion, our results underscore the importance of thermodynamic amplification in shaping future frontal precipitation. While large-scale circulation changes modulate event occurrence, thermodynamic changes, especially increased atmospheric moisture, dominate the intensification of frontal extremes, consistent with the robust physical expectation that heavy precipitation strengthens as the atmosphere warms. By contrast, dynamical circulation changes are less well constrained and contribute more to projection uncertainty, so our confidence is higher in the thermodynamic than in the dynamical component (IPCC, 2023; Li et al., 2025). Together, these findings establish the physical mechanisms behind future changes in frontal weather extremes and strengthen confidence in regional climate impact assessments and adaptation planning.

The extreme events defined here using a 500-day return period are still considered moderate, as the most relevant impacts are typically associated with much rarer and more intense precipitation events (Schär et al., 2016). More detailed process-based analyses of such extreme weather events would require very long time series, which in turn necessitates single-model large-ensemble (SMILE) simulations with at least 6-hourly resolution (Maraun et al., 2025) and CMIP data at hourly resolution to adequately capture the relevant dynamic drivers. Furthermore, convection-permitting models, which explicitly resolve convection within frontal systems and may therefore project different changes in frontal circulation and precipitation intensity (Coppola et al., 2020), need to be performed over larger domains to be applicable to studies of synoptic-scale weather phenomena. Incorporating such simulations in future work would provide a more comprehensive assessment of both thermodynamic and dynamic contributions to extreme precipitation.

Code and data availability. The CMIP6 and EURO-CORDEX data can be accessed from the Earth System Grid Federation (ESGF) nodes (e.g., https://esgf-metagrid.cloud.dkrz.de/search). The data used to produce the figures of this manuscript is available at https://doi.org/10.5281/zenodo.19133794. The code used in this study is available at https://wegcgitlab.uni-graz.at/ars/INTERACT_publishing

Author contributions. AS developed the methodology, carried out the data acquisition and analysis, and wrote the manuscript. DM conceived the project idea. All authors contributed to the interpretation of the results and provided feedback on the manuscript.

https://doi.org/10.5194/egusphere-2026-1712
Preprint. Discussion started: 15 April 2026

Competing interests. The authors declare that they have no conflict of interest.

Acknowledgements. This research was funded by the Austrian Science Fund (FWF) in course of the INTERACT Project (Interactions across scales shaping frontal weather extremes in a changing climate) (I 4831-N). We further want to thank our scientific advisory board member Stephan Pfahl for supporting our research.

https://doi.org/10.5194/egusphere-2026-1712
Preprint. Discussion started: 15 April 2026

References

Bjerknes, J. and Solberg, H.: Life Cycle of cyclones and the polar front theory of atmospheric circulation, Geofysiske. Publikationer, 3, 1922.

Boutle, I. A., Belcher, S. E., and Plant, R. S.: Moisture transport in midlatitude cyclones, Quarterly Journal of the Royal Meteorological Society, 137, 360–373, https://doi.org/10.1002/qj.783, 2011.

Browning, K. A.: Organization of Clouds and Precipitation in Extratropical Cyclones, in: Extratropical Cyclones, edited by Newton, C. W. and Holopainen, E. O., pp. 129–153, American Meteorological Society, Boston, MA, ISBN 978-1-944970-33-8, https://doi.org/10.1007/978-1-944970-33-8_8, 1990.

Browning, K. A. and Monk, G. A.: A Simple Model for the Synoptic Analysis of Cold Fronts, Quarterly Journal of the Royal Meteorological Society, 108, 435–452, https://doi.org/10.1002/qj.49710845609, 1982.

Browning, K. A. and Pardoe, C. W.: Structure of low-level jet streams ahead of mid-latitude cold fronts, Quarterly Journal of the Royal Meteorological Society, 99, 619–638, https://doi.org/10.1002/qj.49709942204, 1973.

Byrne, M. P. and O'Gorman, P. A.: Understanding Decreases in Land Relative Humidity with Global Warming: Conceptual Model and GCM Simulations, Journal of Climate, 29, 9045–9061, https://doi.org/10.1175/JCLI-D-16-0351.1, 2016.

Catto, J. L. and Pfahl, S.: The importance of fronts for extreme precipitation, Journal of Geophysical Research: Atmospheres, 118, 10,791–10,801, https://doi.org/10.1002/jgrd.50852, 2013.

Catto, J. L., Shaffrey, L. C., and Hodges, K. I.: Can Climate Models Capture the Structure of Extratropical Cyclones?, Journal of Climate, 23, 1621–1635, https://doi.org/10.1175/2009JCLI3318.1, 2010.

Catto, J. L., Nicholls, N., Jakob, C., and Shelton, K. L.: Atmospheric fronts in current and future climates, Geophysical Research Letters, 41, 7642–7650, https://doi.org/10.1002/2014GL061943, 2014.

Catto, J. L., Madonna, E., Joos, H., Rudeva, I., and Simmonds, I.: Global Relationship between Fronts and Warm Conveyor Belts and the Impact on Extreme Precipitation*, Journal of Climate, 28, 8411–8429, https://doi.org/10.1175/JCLI-D-15-0171.1, 2015.

Collins, M., Minobe, S., Barreiro, M., Bordoni, S., Kaspi, Y., Kuwano-Yoshida, A., Keenlyside, N., Manzini, E., O'Reilly, C. H., Sutton, R., Xie, S.-P., and Zolina, O.: Challenges and opportunities for improved understanding of regional climate dynamics, Nature Climate Change, 8, 101–108, https://doi.org/10.1038/s41558-017-0059-8, 2018.

Coppola, E., Sobolowski, S., Pichelli, E., Raffaele, F., Ahrens, B., Anders, I., Ban, N., Bastin, S., Belda, M., Belusic, D., Caldas-Alvarez, A., Cardoso, R. M., Davolio, S., Dobler, A., Fernandez, J., Fita, L., Fumiere, Q., Giorgi, F., Goergen, K., Güttler, I., Halenka, T., Heinzeller, D., Hodnebrog, , Jacob, D., Kartsios, S., Katragkou, E., Kendon, E., Khodayar, S., Kunstmann, H., Knist, S., Lavín-Gullón, A., Lind, P., Lorenz, T., Maraun, D., Marelle, L., Van Meijgaard, E., Milovac, J., Myhre, G., Panitz, H.-J., Piazza, M., Raffa, M., Raub, T., Rockel, B., Schär, C., Sieck, K., Soares, P. M. M., Somot, S., Srnec, L., Stocchi, P., Tölle, M. H., Truhetz, H., Vautard, R., De Vries, H., and Warrach-Sagi, K.: A first-of-its-kind multi-model convection permitting ensemble for investigating convective phenomena over Europe and the Mediterranean, Climate Dynamics, 55, 3–34, https://doi.org/10.1007/s00382-018-4521-8, 2020.

Coronese, M., Lamperti, F., Keller, K., Chiaromonte, F., and Roventini, A.: Evidence for sharp increase in the economic damages of extreme natural disasters, Proceedings of the National Academy of Sciences, 116, 21 450–21 455, https://doi.org/10.1073/pnas.1907826116, 2019.

Crawford, A., McCrystall, M., and Loeb, N.: A Decomposition of the Key Drivers of Current and Future Northern Hemisphere Cyclone-Associated Precipitation Trends, Journal of Climate, 38, 3075–3092, https://doi.org/10.1175/JCLI-D-24-0453.1, 2025.

Doswell, C. A., Brooks, H. E., and Maddox, R. A.: Flash Flood Forecasting: An Ingredients-Based Methodology, Weather and Forecasting, 11, 560–581, https://doi.org/10.1175/1520-0434(1996)011<0560:FFFAIB>2.0.CO;2, 1996.

https://doi.org/10.5194/egusphere-2026-1712
Preprint. Discussion started: 15 April 2026

Dottori, F., Szewczyk, W., Ciscar, J.-C., Zhao, F., Alfieri, L., Hirabayashi, Y., Bianchi, A., Mongelli, I., Frieler, K., Betts, R. A., and Feyen, L.: Increased human and economic losses from river flooding with anthropogenic warming, Nature Climate Change, 8, 781–786, https://doi.org/10.1038/s41558-018-0257-z, 2018.

Emori, S. and Brown, S. J.: Dynamic and thermodynamic changes in mean and extreme precipitation under changed climate, Geophysical Research Letters, 32, 2005GL023 272, https://doi.org/10.1029/2005GL023272, 2005.

Eyring, V., Bony, S., Meehl, G. A., Senior, C. A., Stevens, B., Stouffer, R. J., and Taylor, K. E.: Overview of the Coupled Model Intercomparison Project Phase 6 (CMIP6) experimental design and organization, Geoscientific Model Development, 9, 1937–1958, https://doi.org/10.5194/gmd-9-1937-2016, 2016.

Eyring, V., Cox, P. M., Flato, G. M., Gleckler, P. J., Abramowitz, G., Caldwell, P., Collins, W. D., Gier, B. K., Hall, A. D., Hoffman, F. M., Hurtt, G. C., Jahn, A., Jones, C. D., Klein, S. A., Krasting, J. P., Kwiatkowski, L., Lorenz, R., Maloney, E., Meehl, G. A., Pendergrass, A. G., Pincus, R., Ruane, A. C., Russell, J. L., Sanderson, B. M., Santer, B. D., Sherwood, S. C., Simpson, I. R., Stouffer, R. J., and Williamson, M. S.: Taking climate model evaluation to the next level, Nature Climate Change, 9, 102–110, https://doi.org/10.1038/s41558-018-0355-y, 2019.

Feng, S. and Fu, Q.: Expansion of global drylands under a warming climate, Atmospheric Chemistry and Physics, 13, 10 081–10 094, https://doi.org/10.5194/acp-13-10081-2013, 2013.

Field, C. B., Barros, V., Stocker, T. F., and Dahe, Q., eds.: Managing the Risks of Extreme Events and Disasters to Advance Climate Change Adaptation: Special Report of the Intergovernmental Panel on Climate Change, Cambridge University Press, 1 edn., ISBN 978-1-107-02506-6 978-1-107-60780-4 978-1-139-17724-5, https://doi.org/10.1017/CBO9781139177245, 2012.

Folland, C. K., Karl, T. R., Christy, J. R., Clark, R. A., Gruza, G. V., Jouzel, J., Mann, M. E., Oerlemans, J., Salinger, M. J., and Wang, S.-W.: Observed Climate Variability and Change, in: Climate Change 2001: The Scientific Basis. Contribution of Working Group I to the Third Assessment Report of the Intergovernmental Panel on Climate Change [Houghton, J.T.,Y. Ding, D.J. Griggs, M. Noguer, P.J. van der Linden, X. Dai, K. Maskell, and C.A. Johnson (eds.)], Cambridge University Press, Cambridge ; New York, 2001.

Harvey, B. J., Cook, P., Shaffrey, L. C., and Schiemann, R.: The Response of the Northern Hemisphere Storm Tracks and Jet Streams to Climate Change in the CMIP3, CMIP5, and CMIP6 Climate Models, Journal of Geophysical Research: Atmospheres, 125, https://doi.org/10.1029/2020jd032701, 2020.

Heitmann, K., Sprenger, M., Binder, H., Wernli, H., and Joos, H.: Warm conveyor belt characteristics and impacts along the life cycle of extratropical cyclones: case studies and climatological analysis based on ERA5, Weather and Climate Dynamics, 5, 537–557, https://doi.org/10.5194/wcd-5-537-2024, 2024.

Hewson, T. D.: Objective fronts, Meteorological Applications, 5, 37–65, https://doi.org/10.1017/S1350482798000553, 1998.

Hewson, T. D. and Titley, H. A.: Objective identification, typing and tracking of the complete life-cycles of cyclonic features at high spatial resolution: OBJECTIVE IDENTIFICATION, TYPING AND TRACKING OF THE COMPLETE LIFE-CYCLES OF CYCLONIC FEATURES, Meteorological Applications, 17, 355–381, https://doi.org/10.1002/met.204, 2010.

Hénin, R., Ramos, A. M., Schemm, S., Gouveia, C. M., and Liberato, M. L. R.: Assigning precipitation to mid-latitudes fronts on subdaily scales in the North Atlantic and European sector: Climatology and trends, International Journal of Climatology, 39, 317–330, https://doi.org/10.1002/joc.5808, 2019.

IPCC: Climate Change 2021 – The Physical Science Basis: Working Group I Contribution to the Sixth Assessment Report of the Intergovernmental Panel on Climate Change, Cambridge University Press, 1 edn., ISBN 978-1-009-15789-6, https://doi.org/10.1017/9781009157896, 2023.

https://doi.org/10.5194/egusphere-2026-1712
Preprint. Discussion started: 15 April 2026

Jacob, D., Petersen, J., Eggert, B., Alias, A., Christensen, O. B., Bouwer, L. M., Braun, A., Colette, A., Déqué, M., Georgievski, G., Georgopoulou, E., Gobiet, A., Menut, L., Nikulin, G., Haensler, A., Hempelmann, N., Jones, C., Keuler, K., Kovats, S., Kröner, N., Kotlarski, S., Kriegsmann, A., Martin, E., Van Meijgaard, E., Moseley, C., Pfeifer, S., Preuschmann, S., Radermacher, C., Radtke, K., Rechid, D., Rounsevell, M., Samuelsson, P., Somot, S., Soussana, J.-F., Teichmann, C., Valentini, R., Vautard, R., Weber, B., and Yiou, P.: EURO-CORDEX: new high-resolution climate change projections for European impact research, Regional Environmental Change, 14, 563–578, https://doi.org/10.1007/s10113-013-0499-2, 2014.

Jenkner, J., Sprenger, M., Schwenk, I., Schwierz, C., Dierer, S., and Leuenberger, D.: Detection and climatology of fronts in a high-resolution model reanalysis over the Alps, Meteorological Applications, pp. n/a–n/a, https://doi.org/10.1002/met.142, 2009.

Knutti, R., Furrer, R., Tebaldi, C., Cermak, J., and Meehl, G. A.: Challenges in Combining Projections from Multiple Climate Models, Journal of Climate, 23, 2739–2758, https://doi.org/10.1175/2009JCLI3361.1, 2010.

Konstali, K., Spengler, T., Spensberger, C., and Sorteberg, A.: Atmospheric Fronts Drive Future Changes in Extratropical Extreme Precipitation, Geophysical Research Letters, 52, e2025GL116 032, https://doi.org/10.1029/2025GL116032, 2025.

Li, C., Liu, J., Du, F., Zwiers, F. W., and Feng, G.: Increasing certainty in projected local extreme precipitation change, Nature Communications, 16, 850, https://doi.org/10.1038/s41467-025-56235-9, 2025.

Liu, Y., Garcia, M., Zhang, C., and Tang, Q.: Recent decrease in summer precipitation over the Iberian Peninsula closely links to reduction in local moisture recycling, Hydrology and Earth System Sciences, 26, 1925–1936, https://doi.org/10.5194/hess-26-1925-2022, 2022.

Maraun, D., Shepherd, T. G., Widmann, M., Zappa, G., Walton, D., Gutiérrez, J. M., Hagemann, S., Richter, I., Soares, P. M. M., Hall, A., and Mearns, L. O.: Towards process-informed bias correction of climate change simulations, Nature Climate Change, 7, 764–773, https://doi.org/10.1038/nclimate3418, 2017.

Maraun, D., Schiemann, R., Ossó, A., and Jury, M.: Changes in event soil moisture-temperature coupling can intensify very extreme heat beyond expectations, Nature Communications, 16, 734, https://doi.org/10.1038/s41467-025-56109-0, 2025.

Marotzke, J., Jakob, C., Bony, S., Dirmeyer, P. A., O'Gorman, P. A., Hawkins, E., Perkins-Kirkpatrick, S., Quéré, C. L., Nowicki, S., Paulavets, K., Seneviratne, S. I., Stevens, B., and Tuma, M.: Climate research must sharpen its view, Nature Climate Change, 7, 89–91, https://doi.org/10.1038/nclimate3206, 2017.

O'Gorman, P. A. and Schneider, T.: The physical basis for increases in precipitation extremes in simulations of 21st-century climate change, Proceedings of the National Academy of Sciences, 106, 14 773–14 777, https://doi.org/10.1073/pnas.0907610106, 2009.

Ossó, A., Bladé, I., Karpechko, A., Li, C., Maraun, D., Romppainen-Martius, O., Shaffrey, L., Voigt, A., Woollings, T., and Zappa, G.: Advancing Our Understanding of Eddy-driven Jet Stream Responses to Climate Change – A Roadmap, Current Climate Change Reports, 11, 2, https://doi.org/10.1007/s40641-024-00199-3, 2024.

O'Gorman, P. A.: Precipitation Extremes Under Climate Change, Current Climate Change Reports, 1, 49–59, https://doi.org/10.1007/s40641-015-0009-3, 2015.

Pfahl, S., O'Gorman, P. A., and Fischer, E. M.: Understanding the regional pattern of projected future changes in extreme precipitation, Nature Climate Change, 7, 423–427, https://doi.org/10.1038/nclimate3287, 2017.

Priestley, M. D. K. and Catto, J. L.: Future changes in the extratropical storm tracks and cyclone intensity, wind speed, and structure, Weather and Climate Dynamics, 3, 337–360, https://doi.org/10.5194/wcd-3-337-2022, 2022.

Rüdisühli, S., Sprenger, M., Leutwyler, D., Schär, C., and Wernli, H.: Attribution of precipitation to cyclones and fronts over Europe in a kilometer-scale regional climate simulation, Weather and Climate Dynamics, 1, 675–699, https://doi.org/10.5194/wcd-1-675-2020, 2020.

https://doi.org/10.5194/egusphere-2026-1712
Preprint. Discussion started: 15 April 2026

Schaffer, A., Lichtenegger, T., Truhetz, H., Ossó, A., Martínez-Alvarado, O., and Maraun, D.: Drivers of Cold Frontal Hourly Extreme Precipitation: A Climatological Study Over Europe, Geophysical Research Letters, 51, e2024GL111 025, https://doi.org/10.1029/2024GL111025, 2024.

Schaffer, A., Lichtenegger, T., Ossó, A., and Maraun, D.: Resolution dependence and biases in cold and warm frontal heavy precipitation over Europe in CMIP6 and EURO-CORDEX models, Weather and Climate Dynamics, 6, 1815–1830, https://doi.org/10.5194/wcd-6-1815-2025, 2025.

Scheff, J. and Frierson, D. M. W.: Robust future precipitation declines in CMIP5 largely reflect the poleward expansion of model subtropical dry zones, Geophysical Research Letters, 39, 2012GL052 910, https://doi.org/10.1029/2012GL052910, 2012.

Schemm, S., Sprenger, M., Martius, O., Wernli, H., and Zimmer, M.: Increase in the number of extremely strong fronts over Europe? A study based on ERA-Interim reanalysis (1979-2014): Extremely Strong Fronts Over Europe, Geophysical Research Letters, 44, 553–561, https://doi.org/10.1002/2016GL071451, 2017.

Schär, C., Ban, N., Fischer, E. M., Rajczak, J., Schmidli, J., Frei, C., Giorgi, F., Karl, T. R., Kendon, E. J., Tank, A. M. G. K., O'Gorman, P. A., Sillmann, J., Zhang, X., and Zwiers, F. W.: Percentile indices for assessing changes in heavy precipitation events, Climatic Change, 137, 201–216, https://doi.org/10.1007/s10584-016-1669-2, 2016.

Shepherd, T. G.: Atmospheric circulation as a source of uncertainty in climate change projections, Nature Geoscience, 7, 703–708, https://doi.org/10.1038/ngeo2253, 2014.

Simpson, I. R., Shaw, T. A., and Seager, R.: A Diagnosis of the Seasonally and Longitudinally Varying Midlatitude Circulation Response to Global Warming, Journal of the Atmospheric Sciences, 71, 2489–2515, https://doi.org/10.1175/JAS-D-13-0325.1, 2014.

Simpson, I. R., McKinnon, K. A., Kennedy, D., Lawrence, D. M., Lehner, F., and Seager, R.: Observed humidity trends in dry regions contradict climate models, Proceedings of the National Academy of Sciences, 121, e2302480 120, https://doi.org/10.1073/pnas.2302480120, 2024.

Taylor, K. E., Stouffer, R. J., and Meehl, G. A.: An Overview of CMIP5 and the Experiment Design, Bulletin of the American Meteorological Society, 93, 485–498, https://doi.org/10.1175/BAMS-D-11-00094.1, 2012.

Trenberth, K. E., Dai, A., Rasmussen, R. M., and Parsons, D. B.: The Changing Character of Precipitation, Bulletin of the American Meteorological Society, 84, 1205–1218, https://doi.org/10.1175/BAMS-84-9-1205, 2003.

Westra, S., Alexander, L. V., and Zwiers, F. W.: Global Increasing Trends in Annual Maximum Daily Precipitation, Journal of Climate, 26, 3904–3918, https://doi.org/10.1175/JCLI-D-12-00502.1, 2013.

Zappa, G., Shaffrey, L. C., Hodges, K. I., Sansom, P. G., and Stephenson, D. B.: A Multimodel Assessment of Future Projections of North Atlantic and European Extratropical Cyclones in the CMIP5 Climate Models*, Journal of Climate, 26, 5846–5862, https://doi.org/10.1175/JCLI-D-12-00573.1, 2013.

https://doi.org/10.5194/egusphere-2026-1712
Preprint. Discussion started: 15 April 2026

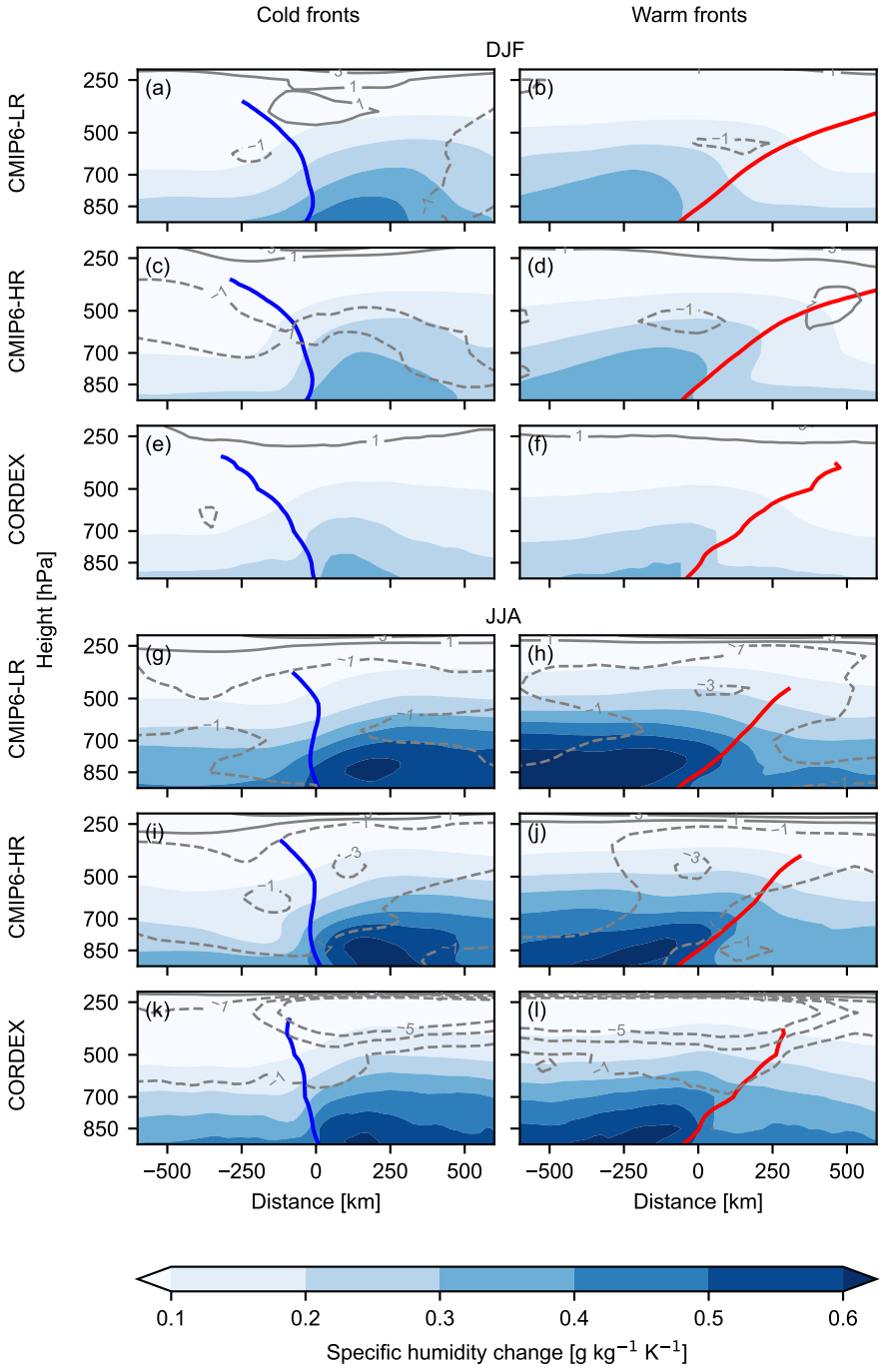

Figure 4. Changes in humidity conditions of frontal composite cross-sections for DJF (a – f) and JJA (g – l). Cold fronts are shown in panels (a, c, e, g, i, k) and warm fronts in (b, d, f, h, j, l). Panels (a, b, g, h) show the low-resolution CMIP6 subset, (c, d, i, j) the high-resolution CMIP6 subset, and (e, f, k, l) EURO-CORDEX. Filled contours indicate the absolute change in specific humidity per degree of global-mean surface temperature change (g kg^{-1} K^{-1}). Gray solid (dashed) contours denote increases (decreases) in relative humidity from -5 to 5 %pt K^{-1} in steps of 2. Blue and red lines mark the mean frontal position based on the TFP zero contour. The x-axis shows cross-frontal distance relative to the detected front at 850 hPa, and the y-axis pressure levels from 925 – 200 hPa.

https://doi.org/10.5194/egusphere-2026-1712
Preprint. Discussion started: 15 April 2026

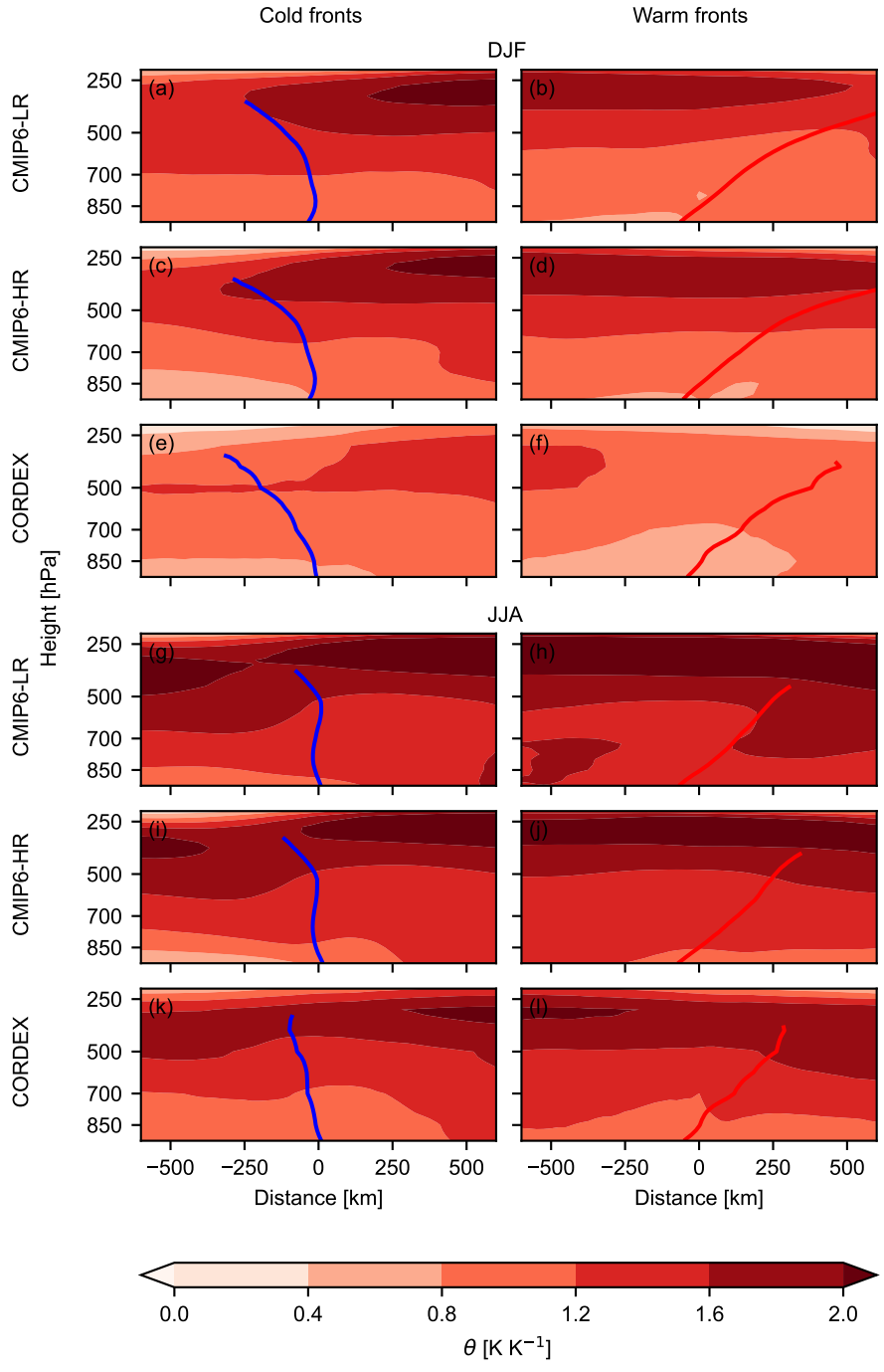

Figure 5. Same as Fig. 1, but depicting the change in potential temperature per degree of global-mean surface temperature change (K K^{-1}).

https://doi.org/10.5194/egusphere-2026-1712
Preprint. Discussion started: 15 April 2026

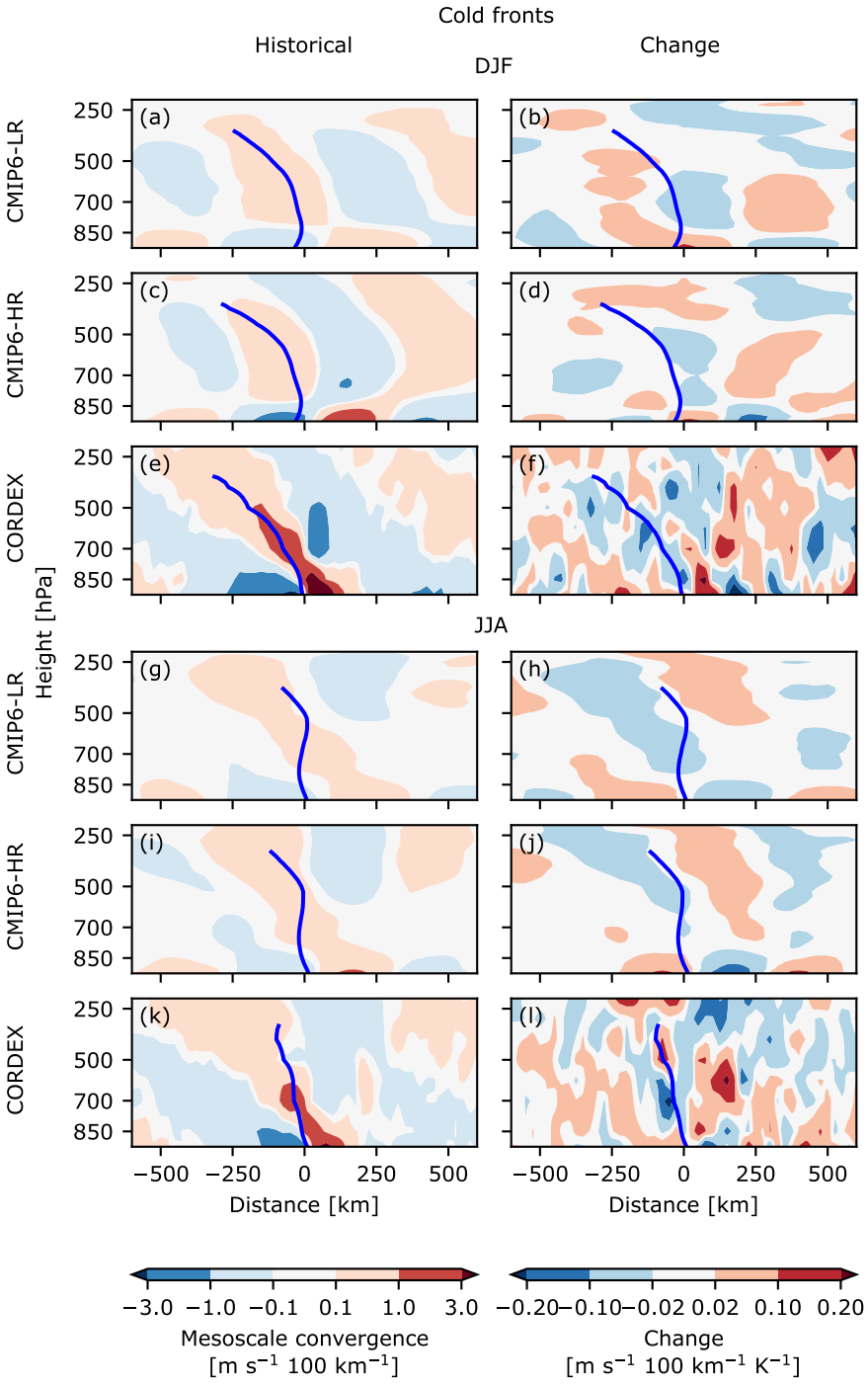

Figure 6. Cold frontal composite cross-sections of mesoscale convergence and the change per degree of ΔGMST for DJF (a – f) and JJA (g – l). Panels (a, b, g, h) show the low-resolution CMIP6 subset, (c, d, i, j) the high-resolution CMIP6 subset, and (e, f, k, l) EURO-CORDEX. Filled contours in the panels (a, c, e, g, i, k) indicate the historical mesoscale convergence (m s^{-1} 100 km^{-1}), (b, d, f, h, j, l) the change per degree of warming (m s^{-1} 100 km^{-1} K^{-1}). Blue lines mark the mean frontal position based on the TFP zero contour. The x-axis shows cross-frontal distance relative to the detected front at 850 hPa, and the y-axis pressure levels from 925 – 200 hPa.

https://doi.org/10.5194/egusphere-2026-1712
Preprint. Discussion started: 15 April 2026

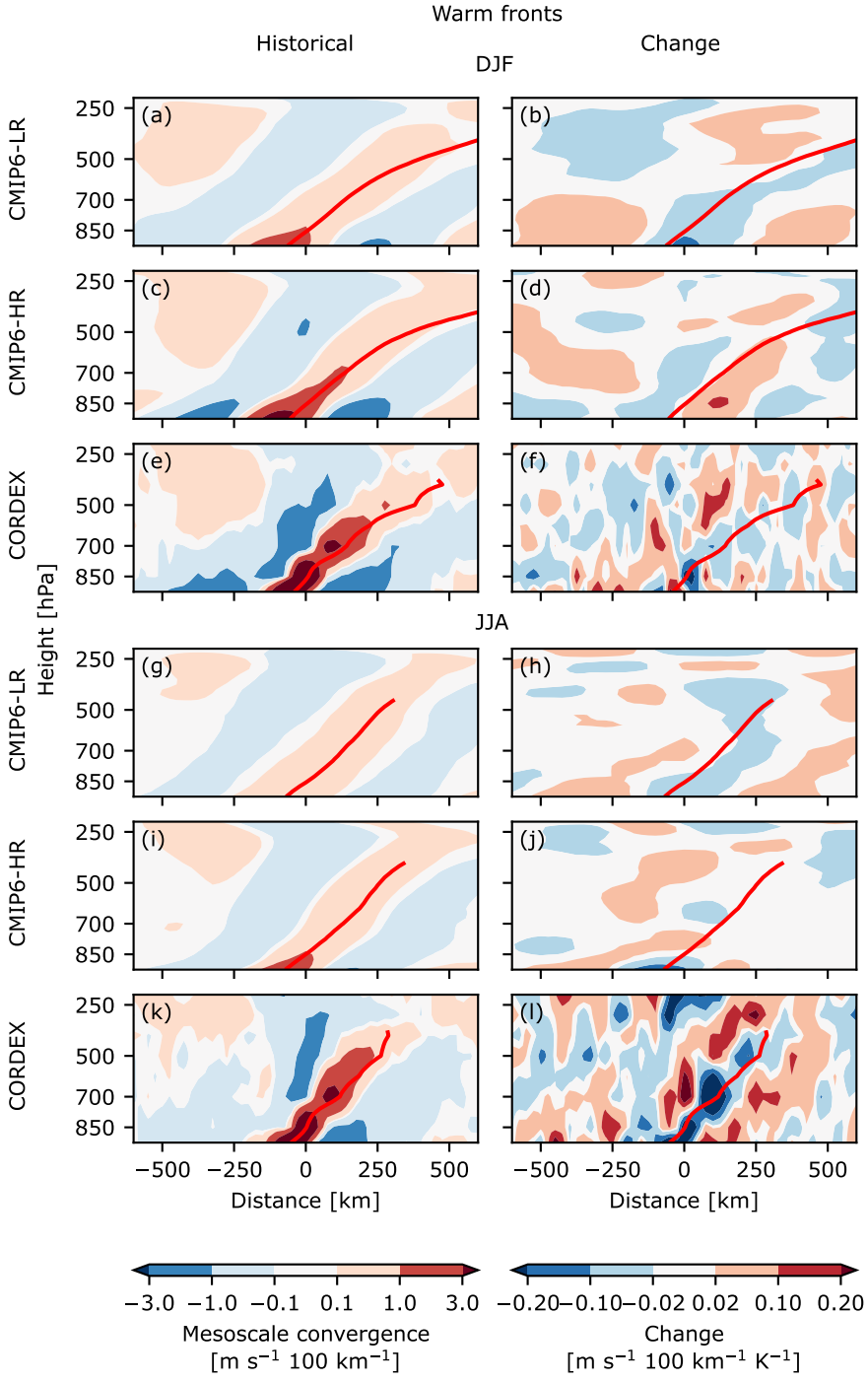

Figure 7. Same as Fig. 6, but in warm frontal cross-sections.

https://doi.org/10.5194/egusphere-2026-1712
Preprint. Discussion started: 15 April 2026

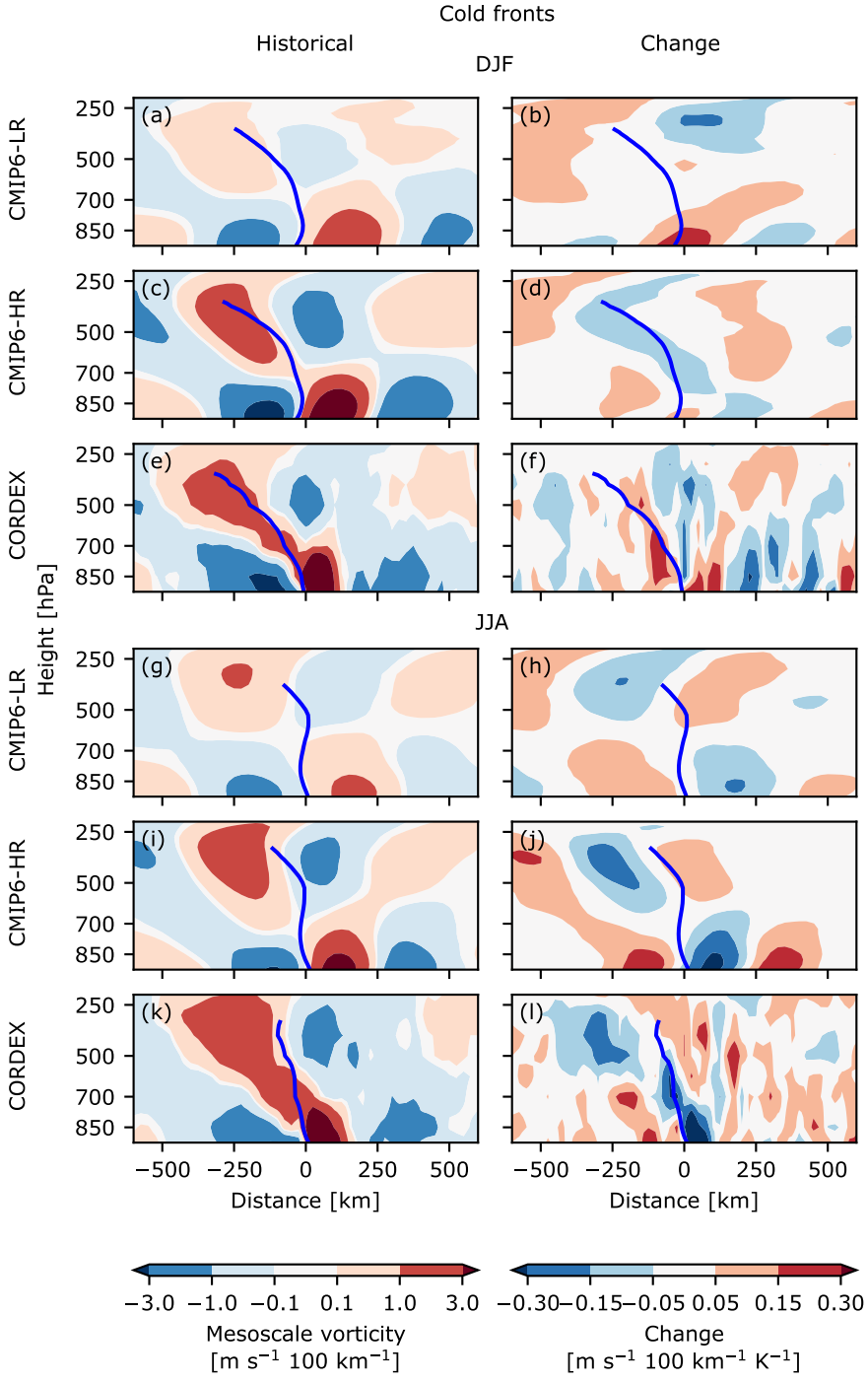

Figure 8. Same as Fig. 6, but depicting mesoscale vorticity and its change in cold fronts.

https://doi.org/10.5194/egusphere-2026-1712
Preprint. Discussion started: 15 April 2026

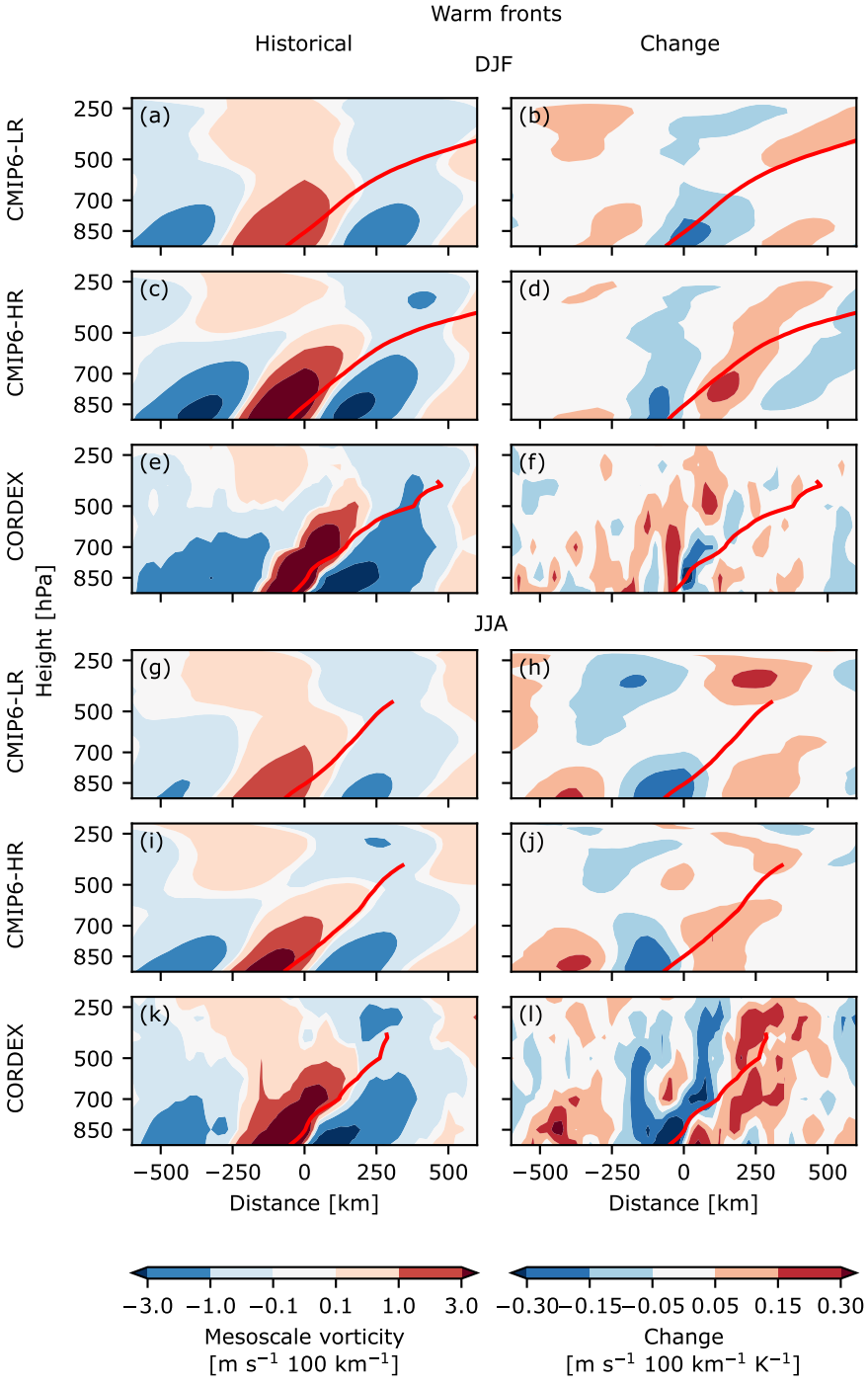

Figure 9. Same as Fig. 6, but depicting mesoscale vorticity and its change in warm fronts.